Electrochimica Acta 133 (2014) 123–131

Contents lists available at ScienceDirect

Electrochimica Acta

journal homepage: www.elsevier.com/locate/electacta

Developing a novel computationally designed impedimetric pregabalin biosensor

Mohammad-Bagher Gholivand[a,*], Ali R. Jalalvand[a,b], Héctor C. Goicoechea[b]

[a] Faculty of Chemistry, Razi University, Kermanshah 671496734, Iran
[b] Laboratorio de Desarrollo Analítico y Quimiometría (LADAQ), Cátedra de Química Analítica I, Universidad Nacional del Litoral, Ciudad Universitaria, CC 242 (S3000ZAA), Santa Fe, Argentina

ARTICLE INFO

Article history:
Received 30 December 2013
Received in revised form 26 March 2014
Accepted 1 April 2014
Available online 16 April 2014

Keywords:
Computationally designed biosensor
Pregabalin
Bovine serum albumin
Graphene

ABSTRACT

A computationally designed impedimetric pregabalin (PGB) biosensor based on immobilization of bovine serum albumin (BSA) onto graphene/glassy carbon electrode (BSA/Gr/GCE) has been developed using initial characterization by computational methods and complementing them by experimental observations. Computational results showed that the BSA hydrophobically binds to Gr which is energetically favorable and leads to the spontaneous formation of the stable nanobiocomposite (BSA/Gr), and also showed that the interaction of PGB with BSA is mainly driven by hydrogen bonding and hydrophobic interactions. The interactions of BSA with Gr and PGB with BSA were also monitored by fluorescence and UVvis spectroscopic techniques, and their results were consistent with the computational results. The electrochemical properties of the fabricated composite electrodes were examined by cyclic voltammetry (CV) scanning electron microscopy (SEM), and electrochemical impedance spectroscopy (EIS) techniques. Besides complementing the computational studies, experimental results showed that the addition of Gr to the surface of the electrode facilitated the electron transfer reactions, and also showed that the presence of BSA inhibits the interfacial electron transfer in some extent due to the non-conductive properties of BSA. The presence of the PGB may form an electroinactive complex with BSA which decelerates the interfacial electron transfer leading to obvious faradaic impedance changes. The faradaic impedance responses were linearly related to PGB concentration between 10.0 nM and 280.0 nM and the limit of detection (LOD) was calculated to be 3.0 nM ($3S_b/b$). Finally, the proposed biosensor was successfully applied to determination of PGB in human serum samples. The results were satisfactory and comparable to those obtained by applying the reference method based on high performance liquid chromatography (HPLC). The results confirmed that the proposed biosensor has good sensitivity, selectivity, stability, repeatability, reproducibility, and regeneration ability for PGB determination.

1. Introduction

Pregabalin (PGB, Fig. 1A) is S-enantiomer of racemic 3-isobutyl-gamma-aminobutyric acid [1], having structure and actions similar to gabapentin. PGB has been used effectively for the treatment of neuropathic pain associated with diabetic peripheral neuropathy, postherpetic neuralgia and other conditions [2]. The analgesic effects of PGB are shown to be mediated by its binding with the α2δ subunit of voltage-gated calcium channels [3–5]. This binding inhibits the influx of Ca^{2+} into the presynaptic terminals, which leads to a subsequent reduction in the release of neurotransmitters such as glutamate and substance P [6,7].

Among biomacromolecules, serum albumin is a soluble protein which commonly serves as a depository and a transport molecule for many exogenous compounds. Bovine serum albumin (BSA, Fig. 1B) is one of the most extensively studied of this group of proteins, particularly because of its structural homology with human serum albumin (HSA). The direct electron transfer between proteins and the electrode surface has received considerable attention, because it can be used in fabricating new generation of biosensor devices. Since redox centers are deeply buried within the proteins molecules, the electron transfer between proteins and the electrode is difficult. Therefore, different substrates could be used to immobilize proteins on the electrode surfaces. Recently, graphene (Gr, Fig. 1C), the 2D carbon material has attracted tremendous attention because of its extraordinary electronic and electrocatalytic

* Corresponding author. Tel.: +98 831 4274557; fax: +98 831 4274559.
E-mail addresses: mbgholivand2013@gmail.com, mbgholivand@yahoo.com (M.-B. Gholivand).

http://dx.doi.org/10.1016/j.electacta.2014.04.017
0013-4686/

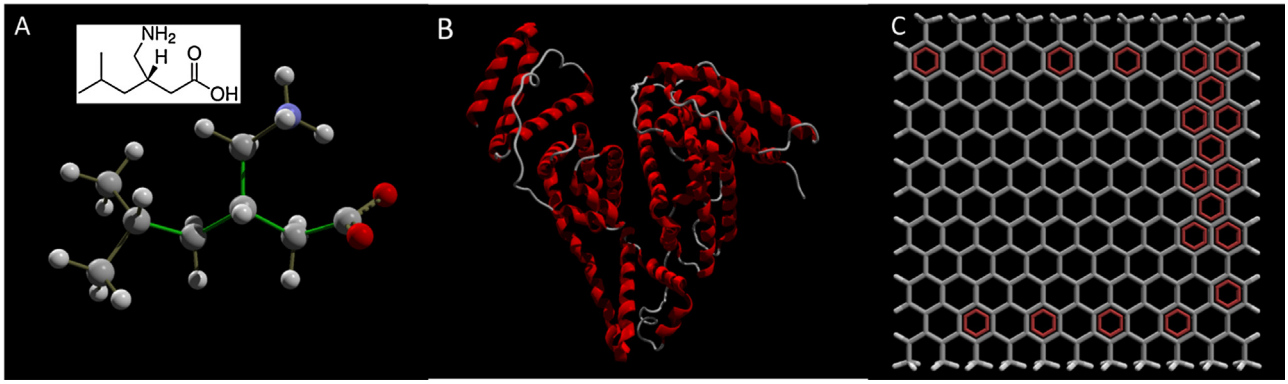

Fig. 1. (A) Molecular structure of PGB represented by ball and stick model, (B) Three-dimensional structure of BSA (chain A) represented by solid ribbon, and (C) Structure of the Gr designed by Nanotube Modeler software and represented by stick model.

properties [8]. The important advantages of Gr based materials such as low cost, mass production [9], high conductivity, large surface area, wide potential window have promoted their further applications [10,11].

The objective of this study is to develop a novel, ultrasensitive, selective and simple impedimetric PGB biosensor with good stability, reproducibility and repeatability for the determination of PGB using unique properties of BSA/Gr nanobiocomposite which can be directly applied in human serum samples without expensive and time-consuming pretreatments. To demonstrate the general design of the BSA/Gr nanostructure based biosensing platform, we first used computational studies for a proof of concept and then completed them by experimental observations. This valuable study describes results obtained by a combination of computational and experimental techniques to develop an ultrasensitive BSA/Gr/GCE biosensor to direct determination of PGB in human serum samples. To the best of our knowledge, this work is the first report on the impedimetric PGB biosensor.

2. Experimental

2.1. Chemicals and solutions

The BSA (M = 66487, free of fatty acids with an electrophoresis grade), and PGB were purchased from Sigma-Aldrich (St. Louis, MO, USA). All other reagents employed were of analytical grade and received from Merck. A concentration of 0.05 M Britton-Robinson buffer solution (BRS) prepared from boric acid, orthophosphoric acid and acetic acid was used to control the pH at 7.40. $[Fe(CN)_6]^{3-/4-}$ solution (redox probe, 5.0 mM) was prepared in BRS (0.05 M, pH 7.4) and used for the measurements. All solutions were prepared by ultrapure water (UPW). The experimental solutions for electrochemical measurements were deoxygenated with N_2 gas for 15.0 min.

Natural graphite (SP-1, Bay Carbon) was treated in strong acid as reported in a modified Hummers method [12]. The resultant graphite oxide was dispersed in the UPW resulting in a dark brown suspension. Graphite oxide was purified by washing with UPW until the pH became neutral and then dispersed in water to obtain a 0.05 wt% dispersion. Graphite oxide was exfoliated to graphene oxide by ultrasonication of the dispersion for 30.0 min. The light brown suspension (graphene oxide) was then separated from the un-exfoliated graphite oxide by centrifugation at 4400.0 rpm for 30.0 min. To obtain Gr, chemical conversion of graphene oxide was employed [13]. Graphene oxide solution (10.0 ml) was mixed with water (10.0 mL), hydrazine solution (10.0 μL, 35 wt% in UPW) and ammonia solution (70.0 μL, 28.0 wt% in UPW) in a conical flask. After shaking for a few seconds, the conical flask was covered and placed in a water bath (100.0 °C) for 2.0 h to produce a dark Gr solution.

2.2. Instrumentation and softwares

Electrochemical experiments were performed using a μ-AutolabIII/FRA2 driven by the Nova 1.8 software. A conventional three-electrode cell was used with a saturated calomel electrode (SCE) as reference electrode, a Pt wire as counter electrode and a bare or modified GCE as working electrode. The SEM experiments were made on a KYKYEM 3200 scanning electron microscope. All fluorescence spectra were measured on a Cary Eclipse fluorescence spectrophotometer equipped with a water bath and a 1.0 cm quartz cell. The UVvis spectra were measured on an Agilent 8453 UVvis Diode-Array spectrophotometer controlled by the Agilent UVvis ChemStation software. A JENWAY-3345 pH-meter equipped with a combined glass electrode was used to pH measurements. Ultrasonication and centrifugation of the solutions were performed, when necessary, using Branson Digital Sonifier (S450D, 500 W, 45% amplitude) and Eppendorf 5702 centrifuge, respectively. High performance liquid chromatography (HPLC) analyzes reported in this study were carried out by a Medical Diagnostic Laboratory in Kermanshah, Iran whose instrument was a P4000 quaternary solvent delivery system equipped with an AS3500 autosampler and column oven (Thermo Separation Products Inc., San Jose, CA, USA). Integration and system parameters were controlled by Spectrasystem PC1000 software (Thermo Separation Products). Separation was performed on a home-made reversed phase analytical column (15 cm × 0.46 cm) packed with Alltima 3C18 (Alltech/Applied Science Group, Breda, The Netherlands) kept at a constant temperature of 30 °C. The column eluate was monitored by a FP920 fluorescence detector (Jasco Corporation, Tokyo, Japan) set at an excitation wavelength of 330 nm and an emission wavelength of 450 nm. Detector gain was set at 100. The mobile phase consisted of a mixture of methanol (8.0 vol. %), acetonitrile (17.5 vol. %) and 20 mM phosphate buffer pH 7.0 (74.5 vol. %) and was delivered isocratically at a flow-rate of 0.8 ml/min. Final pH of the mobile phase was 7.4. The statistical analysis of the sequence of BSA (chain A) was performed using CLC Main Workbench software (Version 6.0). The three-dimensional structure of Gr was generated using Nanotube Modeler software (Fig. 1C). The Gr was then docked to the BSA using Molegro Virtual Docker (MVD) software. The chemical structure of the PGB was constructed by Hyperchem package (Version 8.0), and energy minimization for PGB was performed by AM1 semi empirical method with Polak-Ribiere algorithm until the root mean square gradient of 0.01 kcal mol^{-1}. The MVD software was also employed to generate a docked conformation of PGB with BSA. LIGPLOT [14], a program for automatically plotting protein-ligand

interactions, was used for analyzing the interactions between PGB and BSA. The recorded experimental data was smoothed, when necessary, and converted to matrices by means of several homemade MATLAB (Version 8.1) files. All calculations were run on a DELL XPS laptop (L502X) with Intel Core i7-2630QM 2.0 GHz, 8 GB of RAM and Windows 7-64 as its operating system.

2.3. Preparation of the electrochemical biosensor

The bare GCE was polished with alumina powder and then zinc oxide before modifications. It was then washed with 20.0 ml phosphoric acid solution (0.1 M) to remove the adhered powder, and rinsed with UPW after which the electrode was dried. A known volume (15.0 μL) of Gr solution (0.31 mg mL^{-1}) was casted onto the surface of the clean and dried GCE using a micropipette and dried in a stream of warm air (40.0 °C). The Gr/GCE was then ready for using. The BSA/Gr/GCE was prepared with the following procedure: an 8.0 μL of the BSA (0.15 mg mL^{-1} dissolved in BRS, 0.05 M, pH 7.4) was dripped on the Gr/GCE surface and dried at room temperature to form a stable gel-like film. In some cases the BSA/Gr/GCE was transferred to a PGB solution (25.0 nM) and incubated for 12.0 min. Then, the electrode was extensively rinsed and subjected to electrochemical measurements. To refresh the bare GCE surface it was sonicated in 0.1 M hydrochloric acid for 10.0 min and then acetonitrile for 10.0 min. The electrode surface was dried and then sensed again with the same composition for further experiments.

2.4. Preparation of the real samples

A blank human serum sample (drug-free) was provided by a healthy volunteer, not exposed to any drug for at least 10.0 months. An actual human serum sample was collected from a patient under PGB treatment. According to the method of Han et al. [15], to eliminate protein and other substances, 1.0 mL of human serum sample was placed in a 10.0 mL glass tube and 1.0 ml of 15% (w/v) zinc sulfate solution-acetonitrile (50/40,v/v) was added. The glass tube was vortexed for 20.0 min, maintained at 4.0 °C for 15.0 min followed by centrifugation at 4000.0 rpm for 5.0 min. Then, the supernatant was collected in the same tube and this solution was diluted to 5.0 mL using UPW.

3. Results and discussion

3.1. Computational studies

In order to obtain suitable information related to the interaction of BSA with Gr, the sequence and the crystal structure of BSA (chain A) were theoretically analyzed. The statistical results showed the selected chain of the BSA contains 583.0 amino acids (Fig. 2A), approximately 40.1% were hydrophobic (A, F, G, I, L, M, P, V, and W) and 25.9% were hydrophilic (C, N, Q, S, T, and Y) residues, Fig. 2B. Furthermore, the computational results confirmed that the BSA has approximately the same number of negative and positive groups on its surface, and the calculated isoelectric point was approximately 5.2, Fig. 2C. According to these results, it is reasonable to expect that the interaction of the BSA with Gr will be driven by a combination of hydrophobic and hydrophilic interactions, where the anterior prevails over the latter.

Subsequently, molecular docking studies were performed to identify the potential interaction sites, assuming that the Gr (considered as ligand) would freely rotate around the entire structure of the BSA. Such docking studies allowed us to identify the most likely manner by which Gr was bound to BSA. The docking results with three different views are shown in Fig. 3A-B. An additional advantage of the docking studies is the possibility to identify the residues of BSA that interact with Gr. As can be seen, Gr is surrounded by Glu 207, Ile 202, Gln 203, Glu 206, Arg 208, Phe 205, Lys 204, Lys 350, Ala 254, Glu 478, Thr 477, Glu 357, Glu 358, Lys 474, Thr 473, Glu 470, Pro 467, and Val 468. The interaction of BSA with Gr seems to be dominated by hydrophobic interactions. The binding constant (K_a) and free energy change (ΔG) for the binding of Gr to BSA were $6.78 \times 10^6\ M^{-1}$ and -18.61 kJ M^{-1}, respectively. Therefore, it is also reasonable to expect that the interaction of BSA with Gr will be energetically favorable, leading to the spontaneous formation of the nanobiocomposite. Therefore, such interaction supports the possibility of using a BSA/Gr nanobiocomposite for analytical purposes.

The MVD software was also used to realize the binding mode of PGB at the BSA. The docking results with three different views are shown in Fig. 4A-C. As can be seen, PGB is surrounded by Asn 404, Lys 524, Val 551, Gln 525, Met 547, Leu 528, Phe 550, Ala 527, Phe 508, Val 546, and Leu 531. The K_a and ΔG for the binding of PGB to BSA were calculated to be $3.15 \times 10^5\ M^{-1}$ and -13.30 kJ M^{-1}, respectively. LIGPLOT was used to explore the mode of interaction of PGB with BSA as shown in Fig. 4D. One hydrogen bonding interaction is observed between–NH_2 group of PGB and Lys 524 of BSA, with a distance of 3.0 Å. Based on this information, it is reasonable to expect that the interaction of the PGB with BSA is mainly driven by hydrogen bonding and hydrophobic interactions.

3.2. Experimental studies

3.2.1. Summarized fluorescence quenching and UVvis absorption studies

3.2.1.1. Fluorescence quenching studies. In order to examine the results of computational studies, the interaction of Gr with BSA was also monitored with fluorescence spectroscopy by recording the fluorescence spectra in the BRS (0.05 M, pH 7.4) at three different temperatures including 298.15, 304.15, and 310.15 K, and the representative spectra at 298.15 are shown in Fig. 5A. A gradual increase in Gr concentration in the solutions of BSA caused a decrease in fluorescence intensity without notable changes in the maximum emission wavelength (λ_{max}). In order to further analyze the studied system, the well-known Stern-Volmer equation (Eq. 1) was used to analyze the quenching data.

$$F_0/F = 1 + k_q\tau_0[Q] = 1 + K_{sv}[Q] \quad (1)$$

where F_0 and F represent the fluorescence intensities in the absence and in the presence of quencher (Gr), k_q is the quenching rate constant of the biomolecule, K_{SV} is the dynamic quenching constant, τ_0 is the average lifetime of the molecule, 10^{-8}, and [Q] is the concentration of the Gr [16]. Variations of F_0/F versus [Q] were plotted at 298.15, 304.15, and 310.15 K (not shown), and by linear regression of the plots, K_{SV} values were calculated to be 0.0655, 0.0599, 0.0531 M^{-1}, respectively, decreasing with temperature. Therefore, we concluded that the studied quenching process is a static quenching.

Results of fluorescence spectroscopic measurements can be used to estimate the binding constant of the BSA-Gr hybrid complex by a different form of the Stern-Volmer equation [17]:

$$\log\left(\frac{F_0 - F}{F}\right) = \log K_a + n\log[Q] \quad (2)$$

where F_0, F, and [Q] are the same as in Eq. 1, n is the number of binding sites, and K_a is the binding constant. A plot of log[(F_0 - F)/F] versus log[Q] yields log K_a as the intercept and n as the slope. The K_a and n values obtained at 298.15, 304.15, and 310.15 K are given in Table 1. Values of n were approximately equal to 1.0, which indicated that the existence of one binding sites in BSA for Gr.

The interaction forces between ligands and proteins include hydrogen bonds, van der Waals forces, electrostatic forces, and hydrophobic interaction forces [16]. According to Ross' view [18],

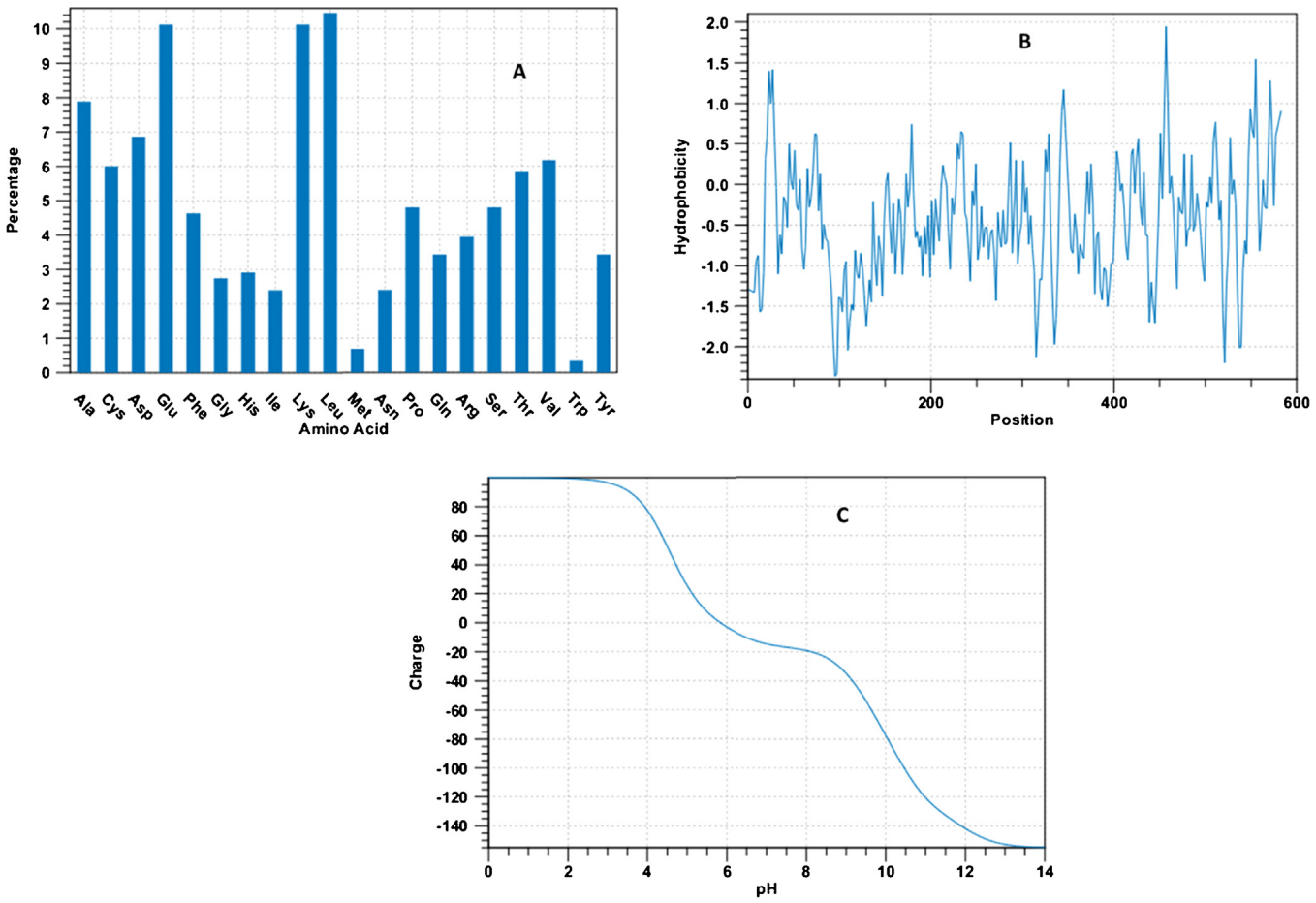

Fig. 2. Results of protein analysis: (A) Amino acid distribution histogram, (B) Hydrophobicity plot, and (C) Electrical charge as a function of pH.

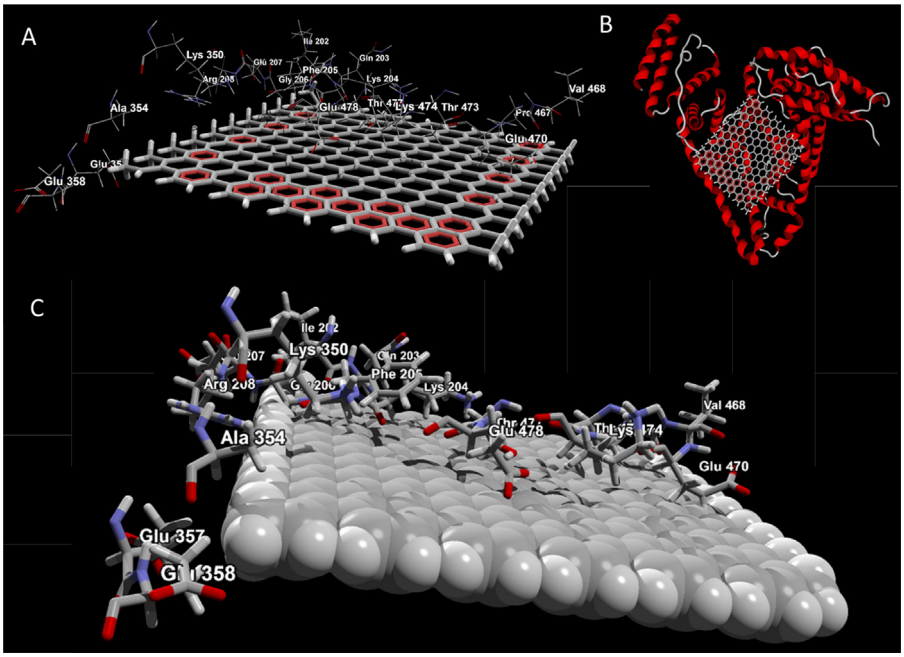

Fig. 3. Computational interaction models of BSA-Gr: (A) BSA residues are represented by stick (thin) and Gr is represented by stick, and (B) BSA is represented by solid ribbon and the Gr is represented by stick model, and (C) BSA residues are represented by stick and Gr is represented using CPK model.

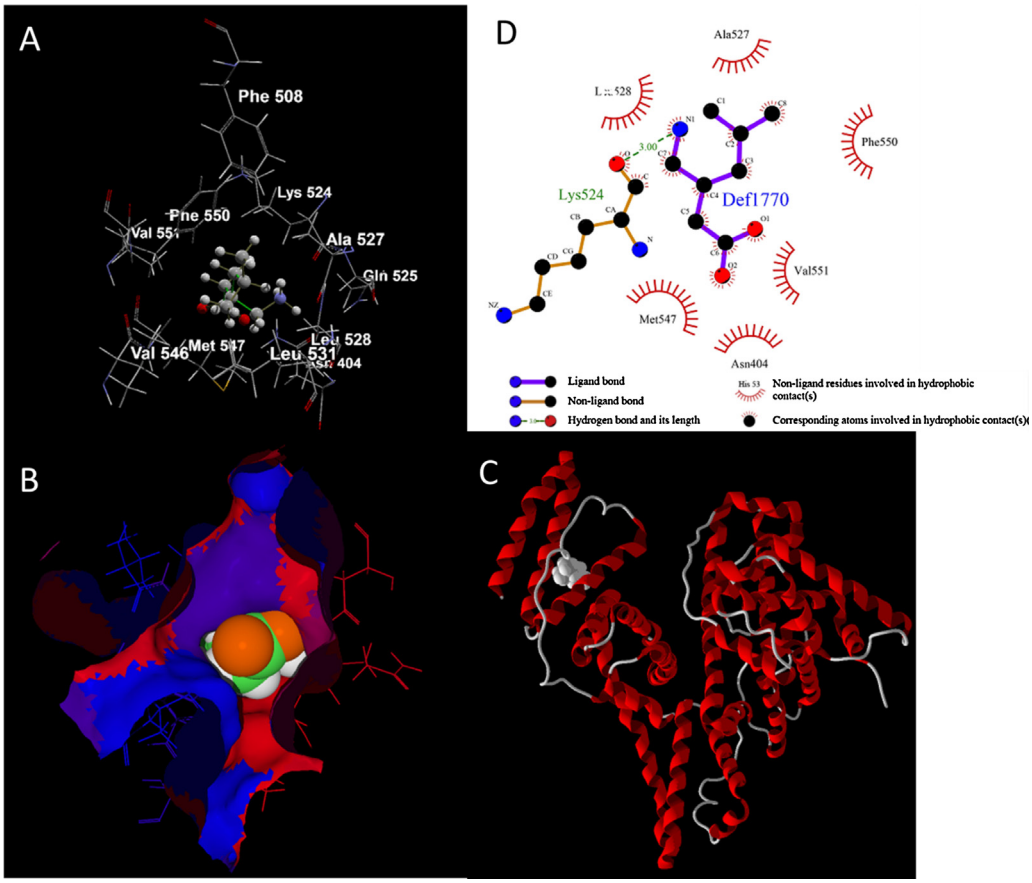

Fig. 4. Computer-generated models of PGB bound to BSA: (A) The residues of BSA are represented by sticks (thin) and the PGB is represented by ball and stick, (B) The binding pocket of protein is represented by hydrophobic interaction and PGB is shown as CPK model, (C) The PGB is shown as CPK and BSA is represented by solid ribbon, and (D) The output of LIGPLOT program.

the signs and magnitudes of thermodynamic parameters (ΔH (enthalpy change), and ΔS (entropy change)) for protein reactions can be used to identify the main forces contributing to protein stability. From the thermodynamics point of view, $\Delta H > 0$ and $\Delta S > 0$ suggest a hydrophobic interaction; $\Delta H < 0$ and $\Delta S < 0$ reflect van der Waals forces or hydrogen bonding; $\Delta H < 0$ and $\Delta S > 0$ suggest electrostatic forces play a key role. When there is no significant change in temperature, the enthalpy of the reaction can be considered as a constant in the formulas by which we calculated the thermodynamic parameters:

$$\ln K = -\frac{\Delta H}{RT} + \frac{\Delta S}{R} \quad (3)$$

where ΔG is free enthalpy change, R is the gas constant 8.314 J mol^{-1} K^{-1}, and T is the temperature. K represents the binding constant at the corresponding temperature. According to Eq. 3, the thermodynamic functions involved in the binding process were calculated and reported in Table 1. The negative sign for ΔG confirms that the binding process is spontaneous. The positive values of ΔS and ΔH revealed the predominance of hydrophobic interactions in the binding of Gr with BSA.

The same procedure (Fig. 5B) was used to study the interaction of PGB with BSA and the results are given in Table 1. The negative values of ΔS and ΔH reveal the predominance of Waals force or hydrogen bonding in the binding of PGB with BSA. With respect to the computational results it could be concluded that the interaction of the PGB with BSA is mainly driven by hydrogen bonding.

3.2.1.2. UVvis absorption studies. UVvis absorption measurement is a simple but efficacious method to investigate structural changes and to confirm complex formation. Therefore, in order to investigate the structural changes in BSA and to confirm the complex formation between Gr and BSA, the UVvis absorption measurements were made [19]. Upon addition of Gr to BSA hyperchromicity occurred in UV absorption spectra of BSA (not shown) which confirmed the absorption of Gr on BSA. The peak at 280.0 nm originates from the π–π^* transition of aromatic amino acid residues such as tryptophan and tyrosine [20]. The micro-environment surrounding

Table 1
Estimated thermodynamic parameters for BSA-Gr and BSA-PGB systems.

T(K)	10^{-6} K_a (L mol^{-1})	n	ΔH(KJ mol^{-1})	ΔS(J mol^{-1}K^{-1})	ΔG(KJ mol^{-1})
BSA-Gr					
298.15	3.9	0.98	36.9	185.7	-18.47
304.15	4.5	1.03			-19.58
310.15	5.3	1.05			-20.69
BSA-PGB					
298.15	24	1.92	-56.16	-143.3	-13.48
304.15	28	1.98			-12.57
310.15	33	2.03			-11.71

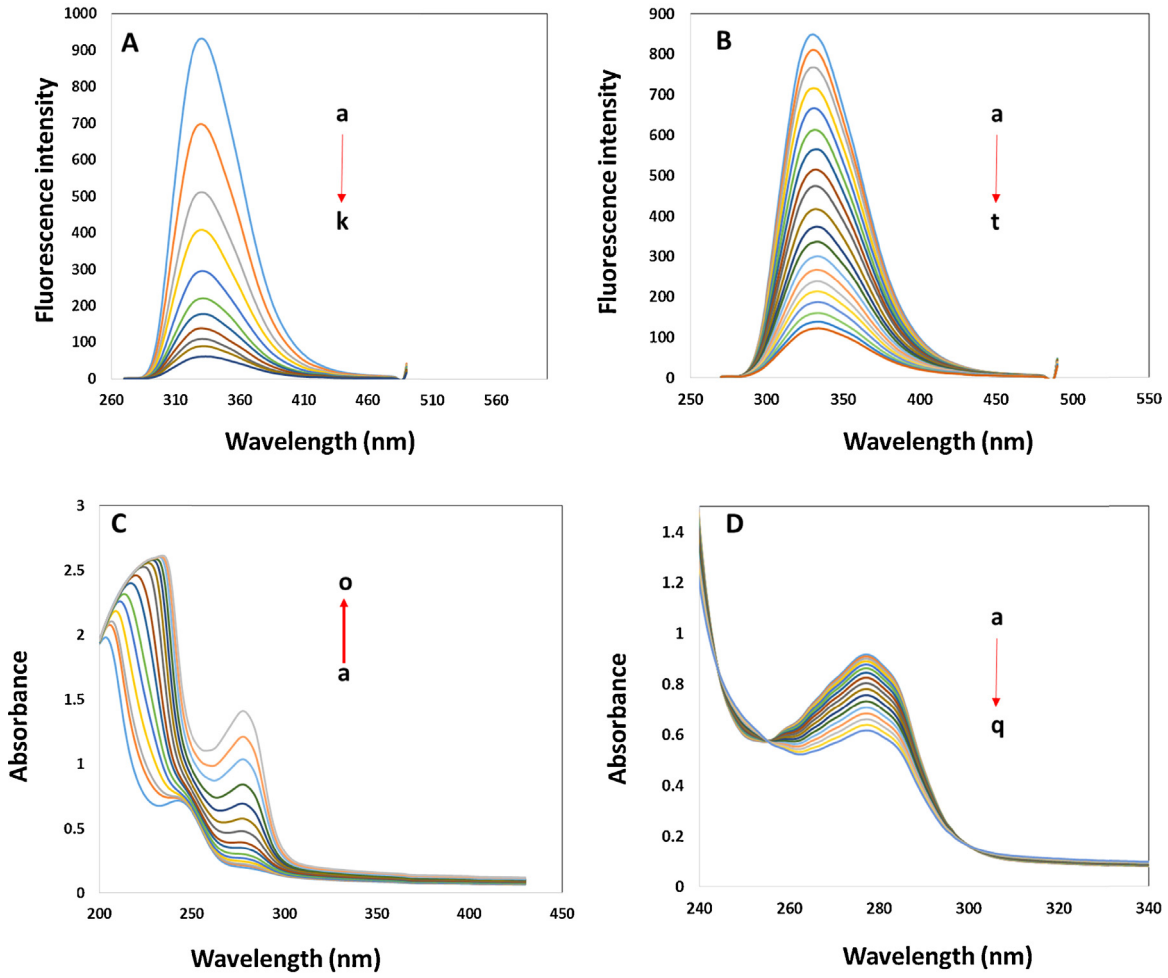

Fig. 5. (A) Fluorescence emission spectra of BSA-Gr system in BRS (0.05 M, pH 7.4) at 298.15 K: (a) free BSA (20.0 μM), and (b-k) BSA 20.0 μM with Gr at 2.5 μM, 5.0 μM, and 10.0-80.0 μM (in steps of 10.0 μM), (B) Fluorescence emission spectra of BSA-PGB system in BRS (0.05 M, pH 7.4) at 298.15 K: (a) free BSA (50.0 μM), and (b-t) BSA 50.0 μM with PGB at 2.5 μM, 5.0-60.0 μM (in steps of 5.0 μM), and 75.0-200.0 μM (in steps of 25.0 μM), (C) UVvis absorption spectra of PGB-BSA system in BRS (0.05 M, pH 7.4): (a) free PGB (7.5 μM), and (b-o) PGB 7.5 μM with BSA at 1.0-7.5 μM (in steps of 0.5 μM), and (D) UVvis absorption spectra of BSA-PGB system in BRS (0.05 M, pH 7.4): (a) free BSA (2.0 μM), and (b-q) BSA 2.0 μM with PGB at 0.5-8.0 μM (in steps of 0.5 μM).

amino acid residues are resolved by molecular conformation of the protein. Furthermore, the UV absorption spectra generate the corresponding change with alteration in micro-environment. Therefore, changes in the spectral characteristics of BSA can be used to judge conformational changes. The intensity of UV absorption spectra of BSA increased noticeably and a blue shift emerges in λ_{max} from 280 nm to 274 nm, conforming the increase in hydrophobicity of amino acid residues. Changes in λ_{max} indicated the change in peptide strand of BSA molecules and hence the change in hydrophobicity. According to these results, we concluded that the interaction between Gr and BSA led to changes in BSA conformation.

In order to investigate the structural changes in BSA upon binding to PGB and to confirm the complex formation between PGB and BSA, the interaction of PGB with BSA was monitored using UVvis absorption measurements. The UVvis absorption studies were carried out by keeping the PGB concentration constant and increasing the BSA concentration (Fig. 5C). It was evident that the intensity of UV absorption of PGB changed with the addition of BSA which are related to complex formation. The UVvis absorption studies were also carried out by keeping the BSA concentration constant and increasing the PGB concentration (Fig. 5D). The absorption peak of BSA at 280.0 nm was found to be decreased and shifted towards higher wavelengths (2.0 nm) in the presence of increased amounts of PGB (Fig. 5D). According to these observations, we proposed that the binding between PGB and BSA led to changes in BSA conformation.

3.2.2. *Morphological studies of the prepared electrodes*

Fig. 6A shows the SEM image of Gr nanosheets on the surface of the GCE. It could be clearly observed that the Gr/GCE showed the typical crumpled and flake structure, indicating that Gr nanosheets had been successfully cast on the electrode GCE surface. When BSA was immobilized onto the Gr/GCE the surface morphology was changed with aggregating the Gr nanosheets (Fig. 6B).

3.2.3. *Optimization studies*

In order to obtain suitable assay results, the effects of some parameters have been investigated in detail. It was found that the amounts of Gr and BSA deposited on the biosensor surface, and incubation time with PGB greatly affected the EIS response of the proposed biosensor. For optimizing the recorded EIS signals, the performance of the biosensors fabricated with different concentrations of Gr (0.05, 0.1, 0.15, 0.21, 0.26, and 0.31 mg mL^{-1}) and BSA (0.4, 0.35, 0.3, 0.25, 0.2, and 0.15 mg mL^{-1}) was studied under different incubation times (42, 36, 30, 24, 18, and 12 min) with the same concentration of 25.0 nM PGB. The changes in R_{ct} (charge transfer resistance) were used to characterize the changes in biosensor surface. The results clearly confirmed that the R_{ct} decreased with

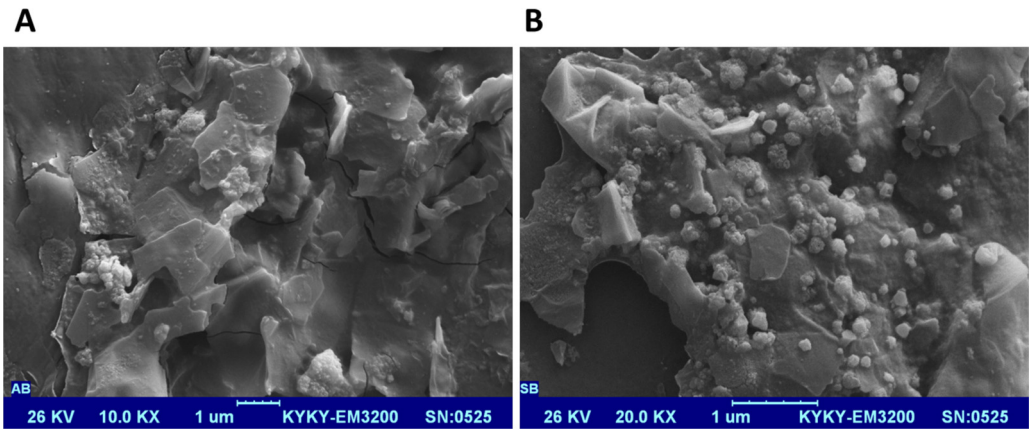

Fig. 6. SEM images of (A) Gr/GCE, and (B) BSA/Gr/GCE.

the increase of amount of Gr when the concentration of Gr was 0.31 mg mL^{-1} (Fig. 7A). Therefore, 0.31 mg mL^{-1} Gr was chosen as the optimized concentration of Gr for the next measurements. Then, effects of amount of BSA on Gr/GCE surface and incubation time of BSA/Gr/GCE with PGB were investigated. It was observed that the R_{ct} decreased with the decrease of both amount of BSA (Fig. 7B) and incubation time (Fig. 7C), when the concentration of BSA and incubation time were 0.15 mg mL^{-1} and 12.0 min, respectively. Therefore, these optimized values were used for the next measurements.

3.2.4. Electrochemical studies

The CVs of 5.0 mM $[Fe(CN)_6]^{3-/4-}$ in BRS 0.05 M, pH 7.4 at a scan rate of 50.0 mV s^{-1} on bare GCE, Gr/GCE, BSA/Gr/GCE, and also BSA/Gr/GCE incubated with PGB (25.0 nM) for 12.0 min were recorded and are showing in Fig. 8A. A standard redox peak could be observed for the bare GCE (Fig. 8A, curve a). The background currents and the redox peaks' currents of Gr/GCE, and BSA/Gr/GCE (Fig. 8A, curves b and c) are larger than those of bare GCE, which confirmed that they have larger effective surface areas. After modification of the bare GCE with Gr, the peak currents and ΔE_P increased and decreased, respectively, which confirmed the enhancement in the electron transfer rate at the Gr/GCE surface. After modification of the Gr/GCE with BSA, it could be seen that the redox currents of the probe decreased, the peak potentials change a little, and no new peak was observed in the same potential scanning range. Therefore, it can be concluded that the presence of BSA inhibits the interfacial electron transfer in some extent due to the non-conductive properties of BSA. When the BSA/Gr/GCE was further incubated in PGB solution (25.0 nM) for 12.0 min, it could be seen that the redox currents and the ΔE_P decreased and increased, respectively, and no new peak was observed in the same potential scanning range (Fig. 8A, curve d). Therefore, according to these observations, it was proposed that the PGB may form an electroinactive complex with BSA which decelerates the electron transfer of the redox probe.

Change in peak current may be related to the change in the effective surface area of the electrode. Therefore, to investigate this parameter, the surface areas of the prepared electrodes were investigated by the Randles-Sevcik equation (298.15 K), using the redox currents of the redox probe (i_p):

$$i_p = (2.687 \times 10^5) n^{3/2} u^{1/2} D^{1/2} A C \quad (4)$$

where D, the diffusion coefficient of the ferricyanide, was 6.3×10^{-6} cm^2 s^{-1}; n and C represent the transferring electron number and the concentration (mol dm^{-3}) of the ferricyanide, respectively; υ was the scan rate (V s^{-1}); and A was the surface area (cm^2).

The surface areas of the bare GCE, Gr/GCE, BSA/Gr/GCE, and BSA/Gr/GCE incubated with PGB (25.0 nM) for 12.0 min were calculated to be 0.12, 0.61, 0.33, and 0.16 cm^2, respectively.

The EIS can be considered as an effective method for probing the features of interfacial electron-transfer resistance during the modification process. In the Nyquist diagram, the diameter of the

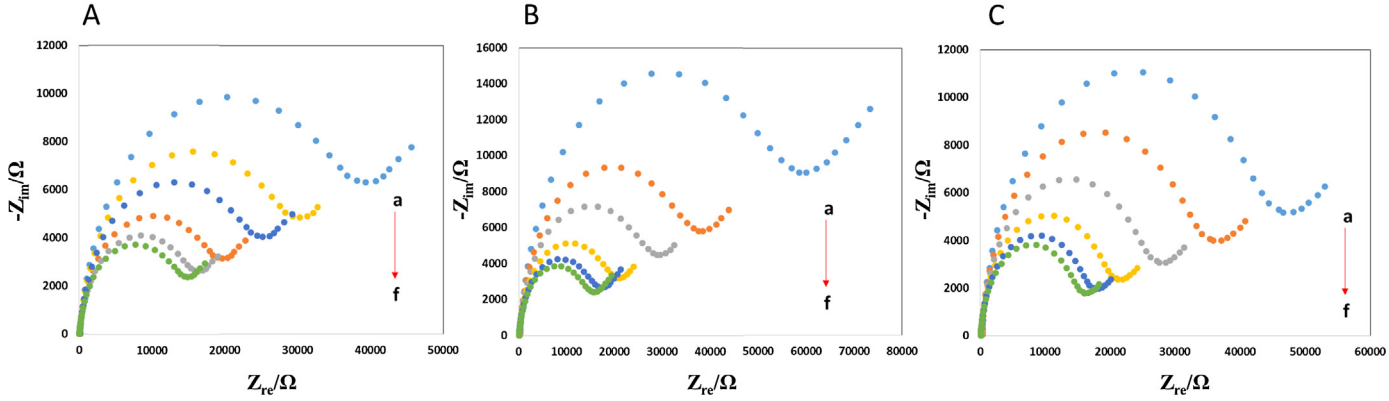

Fig. 7. Optimization procedures in 5.0 mM $[Fe(CN)_6]^{4-/3}$ in BRS 0.05 M, pH 7.4: (A) Effects of Gr concentration on EIS response of the propsed biosensor (Conditions: BSA: 0.15 mg mL^{-1}, PGB: 25.0 nM, incubation time: 12 min, and Gr: 0.05, 0.1, 0.15, 0.21, 0.26, and 0.31 mg mL^{-1} (Curves a-f), (B) Effects of BSA concentration on EIS response of the propsed biosensor (Conditions: Gr: 0.31 mg mL^{-1}, PGB: 25.0 nM, incubation time: 12 min, and BSA: 0.4, 0.35, 0.3, 0.25, 0.2, and 0.15 mg mL^{-1} (Curves a-f), and (C) Effects of incubation time on EIS response of the propsed biosensor (Conditions: Gr: 0.31 mg mL^{-1}, BSA: 0.15 mg mL^{-1}, PGB: 25.0 nM, and incubation time: 42, 36, 30, 24, 18, and 12 min (Curves a-f).

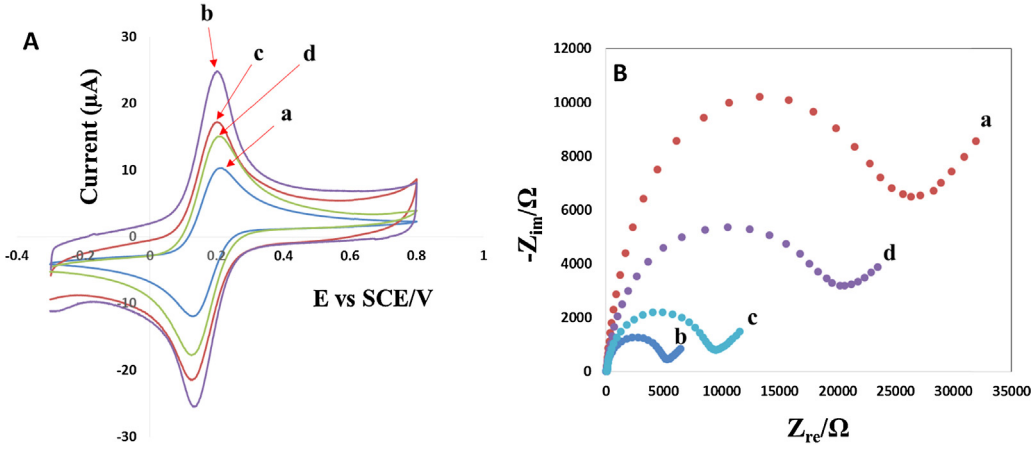

Fig. 8. (A) CVs and (B) EISs of 5.0 mM $[Fe(CN)_6]^{4-/3}$ in BRS 0.05 M, pH 7.4 at a scan rate of 50 mV s^{-1} on (a) bare GCE, (b) Gr/GCE, (c) BSA/Gr/GCE, and (d) BSA/Gr/GCE incubated with PGB (25.0 nM) for 12 min.

semicircle reflects the R_{ct} of redox conversion of $[Fe(CN)_6]^{3-/4-}$ on the electrode surface. In this study, we investigated the changes in R_{ct} during the modification process. The electron transfer process is caused by the presence of the redox couple in the bulk solution and any modification of the electrode surface strongly influences its electrochemical nature, which leads to a change in the R_{ct} value. Fig. 8B, shows the EISs of bare GCE (curve a), Gr/GCE (curve b), BSA/Gr/GCE (curve c), and BSA/Gr/GCE after treatment with PGB (25.0 nM) for 12.0 min (curve d) in the presence of 5.0 mM $[Fe(CN)_6]^{3-/4-}$ in BRS 0.05 M, pH 7.4. As can be seen, a semicircle with R_{ct} about 26.33 kΩ was obtained at the bare GCE. However, the diameter of the semicircle was changed to 5.39 kΩ and 9.82 kΩ by modification of the bare GCE with Gr, and BSA/Gr, respectively, which suggested acceleration and deceleration for $[Fe(CN)_6]^{3-/4-}$ redox reaction due to the presence of Gr and BSA, respectively. A reason for the increase in the R_{ct} value during the modification of Gr/GCE with BSA is that BSA acts as an inert electron layer which hinders the interfacial electron transfer in some extent. In the other hand, by treating the BSA/Gr/GCE with PGB, the interfacial electron resistance increased (20.59 kΩ) coinciding with the CV results. Therefore, the presence of PGB may result in the deactivation of the BSA/Gr/GCE surface by forming an electroinactive complex with BSA which decelerates the interfacial electron transfer and leads to obvious faradaic impedance change.

3.2.5. Analytical applications.

3.2.5.1. PGB determination. Under the optimized condition, the relationship between R_{ct} values and the PGB concentrations was investigated using EIS and the results are showing in Fig. 9. According to the inset of Fig. 9, there is a linear relationship between R_{ct} and PGB concentration over a concentration range from 10.0 nM to 280.0 nM (R^2 0.9894). The linear response obtained by the proposed biosensor in this work indicated that the biosensor could be possibly used in the analysis of real samples. The limit of detection (LOD) of this method was calculated ($3S_b/b$, where S_b is the standard deviation ($n = 7$) of the blanks, and b is the slope of the calibration graph) to be 3.0 nM. Furthermore, the sensitivity of the proposed method was calculated to be 0.15 KΩ nM^{-1} from the slope of the calibration graph, indicating the high sensitivity of the proposed sensing system.

3.2.5.2. Stability, repeatability, reproducibility, and regeneration ability of the developed biosensor. The stability of BSA/Gr/GCE was investigated by measuring a solution of 10.0 nM PGB in 5.0 mM $[Fe(CN)_6]^{3-/4-}$ in BRS (0.05 M, pH 7.4). After fifteen days, the proposed biosensor retained 94.6% of its initial response. After

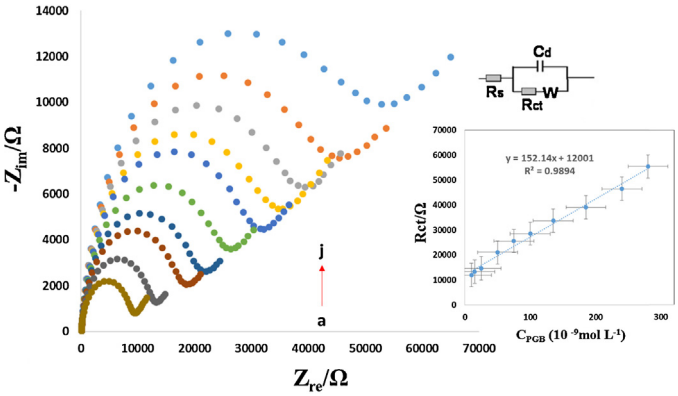

Fig. 9. (A) EIS curves of the BSA/Gr/GCE in 5.0 mM $[Fe(CN)_6]^{3-/4-}$ in BRS 0.05 M, pH 7.4 corresponding to different concentrations of PGB: (a) 0, (b) 10.0 nM, (c) 25.0 nM, (d) 50.0 nM, (e) 100.0 nM, (f) 150.0 nM, (g) 200.0 nM, (h) 225.0 nM, (i) 250.0 nM, and (j) 280.0 nM. Top inset: the equivalent circuit used for fitting the EIS responses of the proposed biosensor. Bottom inset: The corresponding calibration plot of R_{ct} vs. different concentrations of PGB.

one month, the biosensor response decreased about 8.9%. It was observed that the stability of the proposed biosensor was affected by the time of immersing the biosensor in the cell solution. Therefore, the effect of this parameter on the biosensor stability was investigated and it was found that the biosensor didn't show good stability when it continued in contact with the cell solution for more than 6.0 h. Therefore, it is recommended to remove the biosensor from cell solution during the breaks between measurements. The repeatability of the proposed biosensor was investigated for ten times within the same day giving satisfied relative standard deviation (*RSD*) of 3.8%. The reproducibility of the BSA/GR/GCE was examined by recording the EIS responses of six individual biosensors in 5.0 mM $[Fe(CN)_6]^{3-/4-}$ in BRS (0.05 M, pH 7.4) containing 25.0 nM PGB and the *RSD* was got as 4.9%. The above results indicated good stability, repeatability, and reproducibility of the proposed biosensor.

Regeneration ability is another important factor of monitoring the performance of the developed biosensor therefore, regeneration of the developed PGB biosensor was investigated. The electrode possessed 94.1% of its original EIS response in 5.0 mM $[Fe(CN)_6]^{3-/4-}$ in BRS (0.05 M, pH 7.4) containing 25.0 nM PGB when the fabricated biosensor was regenerated 10 times by rinsing the surface of the biosensor with hot UPW for 5 min, followed by rapid cooling in icy bath. It confirms that the proposed

Table 2
Effect of interfering spices on the PGB determination.

Interfering species	Tolerance ratio
Thiourea	0.25×10^2
Dopamine	0.25×10^2
Uric acid	0.25×10^2
Sorbitol	0.25×10^2
Sucrose	2.01×10^2
Fructose	2.01×10^2
Epinephrine	2.01×10^2
Glucose	1.2×10^2
Ascorbic acid	1.2×10^2
Histidine	1.5×10^2
Valine	1.5×10^2
Tryptophan	1.5×10^2
Alanine	1.5×10^2

Table 3
Determination of PGB in human serum samples (n = 3).

Samples	Added (10^{-9}mol L^{-1})	Found (10^{-9}mol L^{-1})	Recovery (%)	HPLC
Serum[h]	20.0	19.7 ± 0.2	98.5	20.0 ± 0.1
	15.0	15.1 ± 0.2	100.7	14.9 ± 0.1
	-	<LOD	-	<LOD
	55.0	53.1 ± 0.8	96.54	55.2 ± 0.3
Serum[p]	-	12.2 ± 0.5	-	-12.0 ± 0.1
	2.0	13.9 ± 0.1	95.0	13.9 ± 0.1
	80.0	94.3 ± 0.6	102.8	91.1 ± 0.3
	10.0	22.4 ± 0.4	103.8	22.1 ± 0.2

[h] Healthy volunteer.
[p] Patient volunteer.

biosensor has good regeneration ability for PGB detection. Therefore, the regeneration of the BSA/Gr/GCE possessed potential for continuous monitoring of target PGB.

3.2.5.3. Interference study. To evaluate the selectivity of the proposed biosensor, some possible interfering species such as thiourea, dopamine, uric acid, sorbitol, sucrose, fructose, glucose, epinephrine, ascorbic acid, histidine, valine, tryptophan and alanine which may be present in real samples, were tested in 5.0 mM $[Fe(CN)_6]^{3-/4-}$ in BRS (0.05 M, pH 7.4) containing PGB (25.0 nM). The results as obtained in terms of tolerance ratios during determination of 25.0 nM of PGB are compiled in Table 2. The tolerance limit was defined as the concentration of added species causing less than ±5 relative error on the determination of 25.0 nM of PGB.

3.2.5.4. Determination of PGB in real samples. To examine the BSA/Gr/GCE's ability to determination of PGB, we tested its ability to detect PGB in human serum samples of both healthy and patient volunteers. Results are shown in Table 3. As can be seen, good recoveries were obtained which suggested that the proposed biosensor was both effective and sensitive for determination of PGB in real samples. The accuracy of the proposed method in this study was also compared with the HPLC results. The results presented in Table 2 confirm that the proposed biosensor shows a good accuracy for determination of PGB in real samples. Therefore, the successful detection of PGB in biological samples as demonstrated here may be straightforward when testing for PGB clinically. Compared with the HPLC method, the proposed biosensor is simple, easily implemented, and has low-cost and fast response. Thus, accurate and successful determination of PGB in biological fluids as demonstrated here may allow one to propose the present biosensor as a promissory, cheap and accessible alternative for the clinical analysis of PGB.

4. Conclusions

In conclusion, a computationally engineered nanobiocomposite based on immobilization of BSA onto GR was used to construct an ultrasensitive impedimetric PGB biosensor. The computational results were confirmed by experimental observations. The proposed biosensor exhibited stable, regenerable, and sensitive functions for PGB determination. The characterizations performed by CV, and EIS suggest that the incubation of BSA/Gr/GCE with PGB significantly decreases the electrode surface area which leads to obvious faradaic impedance changes. The present work not only provides a better understanding of parameters involved in the development of BSA/Gr nanobiocomposite, but also shows the advantages related to the use of computational techniques in developing new and efficient biosensors. The principles used in this study could potentially be used to construct new biosensors in clinical settings for biological fluids.

Acknowledgements

The authors gratefully acknowledge the financial supports of this project by the Razi University Research Council, UNL, CONICET and ANPCyT. The authors would like to thank the reviewers for their insightful comments which led to an improvement of the work.

References

[1] G. Zareba, Pregabalin A new agent for the treatment of neuropathic pain, Drugs Today (Barc) 41 (2005) 509.
[2] P. Ryvlin, Defining success in clinical trials–profiling pregabalin, Eur. J. Neurol. 12 (Suppl. 4) (2005) 12.
[3] M.J. Field, P.J. Cox, E. Stott, H. Melrose, J. Offord, T.Z. Su, S. Bramwell, L. Corradini, S. England, J. Winks, R.A. Kinloch, J. Hendrich, A.C. Dolphin, T. Webb, D. Williams, Identification of the alpha2-delta-1 subunit of voltage-dependent calcium channels as a molecular target for pain mediating theanalgesic actions of pregabalin, Proc. Natl. Acad. Sci. U.S.A. 103 (2006) 17537.
[4] D.J. Martin, D. McClelland, M.B. Herd, K.G. Sutton, M.D. Hall, K. Lee, R.D. Pinnock, R.H. Scott, Gabapentin-mediated inhibition of voltage-activated Ca^{2+} channel currents in cultured sensory neurons is dependent on culture conditions and channel subunit expression, Neuropharmacology 42 (2002) 353.
[5] C.P. Taylor, The biology and pharmacology of calcium channel alpha2-deltaproteins, in: Pfizer Satellite Symposium to the 2003 Society for Neuroscience Meeting, Sheraton New Orleans Hotel, New Orleans, LA November 10, 2003, CNS Drug Rev. 10 (2004) 183.
[6] D.J. Dooley, C.A. Mieske, S.A. Borosky, Inhibition of K(+)-evoked glutamate release from rat neocortical and hippocampal slices by gabapentin, Neurosci. Lett. 280 (2000) 107.
[7] Y.P. Maneuf, J. Hughes, A.T. McKnight, Gabapentin inhibits the substance P-facilitated K(+)-evoked release of [(3)H]glutamate from rat caudial trigeminal nucleus slices, Pain 93 (2001) 191.
[8] A.K. Geim, K.S. Novoselov, The Rise of Graphene, Nature Materials 6 (2007) 183.
[9] M. Pumera, A. Ambrosi, A. Bonanni, E.L.K. Chng, H.L. Poh, Graphene for electrochemical sensing and biosensing, Trends Anal. Chem. 29 (2010) 954.
[10] Y. Shao, J. Wang, H. Wu, J. Liu, I.A. Aksay, Y. Lin, Graphene Based Electrochemical Sensors and Biosensors: A Review, Electroanalysis 22 (2010) 1027.
[11] Y.M. Li, L.H. Tang, J.H. Li, Preparation and electrochemical performance for methanol oxidation of pt/graphene nanocomposites, Electrochem. Commun. 11 (2009) 846.
[12] W.S. Hummers, R.E. Offeman, Preparation of graphitic oxide, J. Am. Chem. Soc. 80 (1958) 1339.
[13] D. Li, M.B. Muller, S. Gilje, R.B. Kaner, G.G. Wallace, Processable aqueous dispersions of graphene nanosheets, Nat. Nano 3 (2008) 101.
[14] A.C. Wallace, R.A. Laskowski, J.M. Thornton, LIGPLOT. A program to generate schematic diagrams of protein-ligand interactions, Protein Eng 8 (1995) 127.
[15] J.H. Suh, Y.Y. Lee, H.J. Lee, M. Kang, Y. Hur, S.N. Lee, D.H. Yang, S.B. Han, Dispersive liquid-liquid microextraction based on solidification of floating organic droplets followed by high performance liquid chromatography for the determination of duloxetine in human plasma, J. Pharm. Biomed. Anal. 75 (2013) 214.
[16] J.R. Lakowicz, Principles of Fluorescence Spectroscopy, Third Edition, Springer, New York, 2006.
[17] Y.J. Hu, Y. Liu, X.-H. Xiao, Investigation of the Interaction between Berberine and Human Serum Albumin, Biomacromolecules 10 (2009) 517.
[18] P.D. Ross, S. Subramanian, Thermodynamics of protein association reactions: Forces contributing to stability, Biochemistry 20 (1981) 3096.
[19] S. Bi, D. Song, Y. Tian, X. Zhou, Z. Liu, H. Zhang, Molecular spectroscopic study on the interaction of tetracyclines with serum albumins, Spectrochim Acta, Part A 61 (2005) 629.
[20] A.N. Glazer, E. Smitth, Studies on the Ultraviolet Difference Spectra of Proteins and Polypeptides, J. Biochem. 236 (1961) 2942.